Int J Adv Manuf Technol (2015) 76:1621–1630
DOI 10.1007/s00170-014-6353-y

ORIGINAL ARTICLE

Effects of channel angles on extrusion-shear for AZ31 magnesium alloy: modeling and experiments

H-J Hu · H Wang · Z-Y Zhai · Y-Y Li · J-Z Fan · Z-W Ou

Received: 6 May 2014 / Accepted: 4 September 2014 / Published online: 23 September 2014

Abstract To improve the industrialization of the severe plastic deformations (SPD) technology for magnesium (Mg) alloy, a new extrusion-shear (ES) process has been explored and widely investigated owing to its potential ability to produce ultra-fine-grained microstructures in Mg alloys. It is crucial to understand the effect of die design on the deformation behavior, strain distribution, and load requirements during ES process. Three-dimensional geometric models with different channel angles (135°, 120°) in the ES dies have been designed. The plastic deformation heterogeneities of ES process with different channel angles have been analyzed from the simulation results. The results can be summarized as follows. The equivalent strains and loads during the whole ES process decrease with the increase of channel angles. The decrease of channel angle could improve the deformation inhomogeneity of ES process. Smaller channel angles could promote the higher cumulative strains and finer subgrains. The analysis results show that finer and more uniform microstructures can be obtained if channel angles in the ES dies are appropriate. It is demonstrated that the predicted results are in good agreement with experiments results and the theoretical calculations. Numerical simulations and experiments could help to understand the deformation behaviors of AZ31 Mg alloy during ES.

Keywords Magnesium alloy · Plastic deformation · Extrusion-shear · Channel angle · Finite element method

H.-J. Hu (✉) · H. Wang · Z.-Y. Zhai · Y.-Y. Li · J.-Z. Fan
College of Material Science and Engineering, Chongqing University of Technology, 400050 Chongqing, China
e-mail: 278368707@qq.com

Z.-W. Ou
The PLA Chongqing Logistics Engineering College, 401311 Chongqing, China

1 Introduction

As the lightest structural material of engineering significance, magnesium (Mg) alloys have attracted considerable recent attention [1, 2]. However, the mechanical properties of Mg alloy are still not high enough, which limits its application in the industry. One of the promising methods for increasing ductility and strength in Mg alloys is through microstructure refinement. A fine-grained material is harder and stronger than one that is coarsely grained because it has a greater total grain boundary area to impede dislocation motion [3, 4]. Severe plastic deformation (SPD) has provided new opportunities for mechanical properties enhancement through grain refinement. Gong et al. investigated the SPD using differential speed rolling on Mg alloys: the grain refinement is achieved and the mechanical properties of Mg alloys are greatly improved [5, 6]. Segal et al. [1] and Matsuyama et al. [7] applied equal channel angular extrusion (ECAE) to obtain Mg alloys with high strength and toughness. The ECAE usually includes more than two steps, and the material endures intricate diversification of forming environments including process temperature and may be oxidized. However, Matsubara et al. [8] pointed out that ECAE could only be applied in the lab-scale processing and preparation for nanocrystalline material; there exist an unbridgeable gap between the experimentation and applications of industry. Recently, Orlov et al. [9] investigated the feasibility of SPD techniques which combine direct extrusion and two steps of equal channel angular pressing in a single process, and process material with an excellent balance of strength and tensile ductility.

In the current research, a new approach of extrusion-shear (ES) is introduced to fabricate Mg alloys which includes two consecutive processes: combination of initial direct extrusion and subsequent successive shearing. The structure of ES die is shown in Fig. 1. The ES die contains three components: extrusion cylinder and direct extrusion zone and two

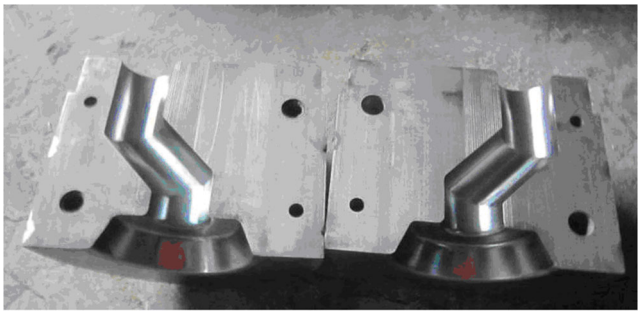

Fig. 1 Structures of ES die

consecutive shearing zones. An oblique angle Φ is located at the intersecting cross-section channel which is called die channel angle. ES process not only makes continuous forming but also allows the various kinds of rods into the desired final dimensions. The authors' research team was engaged in the research studies of the ES process which included initial forward extrusion and shearing process subsequently since 2008 [10]. ES process is well suited for manufacturing long, straight products with a constant cross section and continuous extrusion. ES process can improve workability and strength of Mg alloys by refining the grains.

The design of ES die has not been well known or understood by the public. It is interpreted as that the technology or the mechanism regarding the ES die design and the plastic deformation has not been fully developed yet. In order to understand the behavior of the plastic deformation for ES extrusion, two types of ES dies with different channel angles have been designed and manufactured.

Finite element method (FEM) is one of the important approaches to understand the plastic deformation behaviors [11–13]. FEM-based analysis has been performed to determine the deformation behaviors of materials and estimate the strain and stress distributions [14–17]. The plastic deformation behaviors during ES process are governed mainly by the die geometry parameters, the material itself, and the processing conditions. This study is to numerically analyze the plastic deformation behaviors of AZ31 Mg alloy and predict the strains and extrusion forces during ES process.

Table 1 Simulation and experimental parameters

Channel angle (deg)	120, 135
Billet length (mm)	260
Billet diameter (mm)	80
Container insider diameter (mm)	82
Container outside diameter (mm)	84
Die bearing length (mm)	5
Extrusion ratio	12
Ram speed (mm/s)	20
Friction factor of the container–billet interface	0.4
Friction factor between the billet and die	0.4
Heat transfer coefficient between tooling and billet (N/°C s mm^2)	11
Heat transfer coefficient between tooling/billet and air (N/°C s mm^2)	0.02
Total number of elements for billet	20,000
Mesh density type	Relative
Starting step number	−1
Number of simulation steps	500
Step increment to save	1
Maximum stroke per step	0.1
Master–slave die	Die-billet
Master–slave die	Ram-billet
Relative interference depth	0.7

The two geometric models for ES dies have been constructed in UG software which is meshed and simulated in DEFORM™-3D code. The effects of different die geometries on the strain and stress distributions and deformation inhomogeneity during ES have been investigated. Because the microstructure evolution and mechanical properties of deformed material are directly related to the behavior of plastic deformations, the understanding of the phenomenon associated with the strain development is very important for ES process. Distributions of effective stress and strain, influences of channel angles on the plastic deformation in different zones and flow homogeneity, and maximum strain have been discussed in detail. Experiments for two ES dies with different channel angles have been done to validate the simulation results.

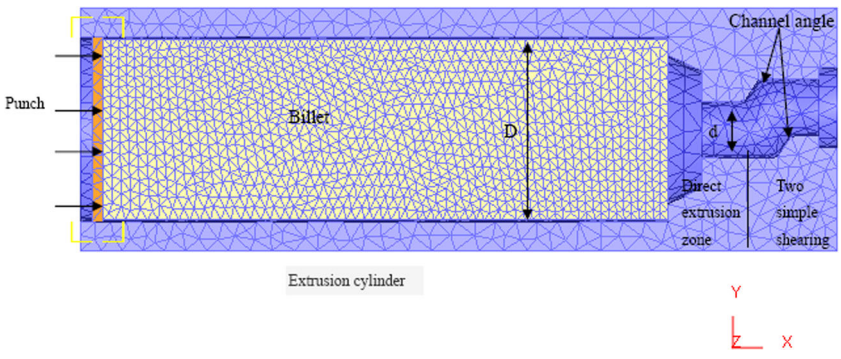

Fig. 2 Schematic diagrams of the three-dimensional FEM modeling for ES die

2 Simulation details

The geometries of die and billet and punch used in the simulations are shown in Fig. 2, and channel angles of ES dies are 120° and 135°, respectively. The radius at the intersection of the two channels is equal to 1 mm, and fillet radius is 3 mm in the geometrical parameters of the ES dies, as can be seen in Fig. 2. The diameter of billet is 80 mm and the diameter of rod is 25 mm. The dimensions of channel diameters for simple shear zone including both the inlet and outlet channels are the same and equal to 25 mm.

Table 1 presents the dimensions, extrusion speed, and temperature parameters used in FEM, which are identical to those applied in ES process experiments. The dies and pressing ram are an H13 tool-steel with the Young's modulus and temperature-dependent conduction on the temperature shown in Fig. 3a, b. The Poisson's ratio (ν) is 0.3. Two distinct geometric models with channel angles 120° and 135° have been analyzed by numerical simulation to reveal the deformation behaviors and their relationship with the design configuration.

The AZ31 is considered as an isotropic elastic–plastic material [19]. The flow stress curves measured in these tests have been corrected and a set of flow stress–strain curves are shown in Fig. 4 as examples. Material property parameters of the AZ31 workpiece are listed in Table 2.

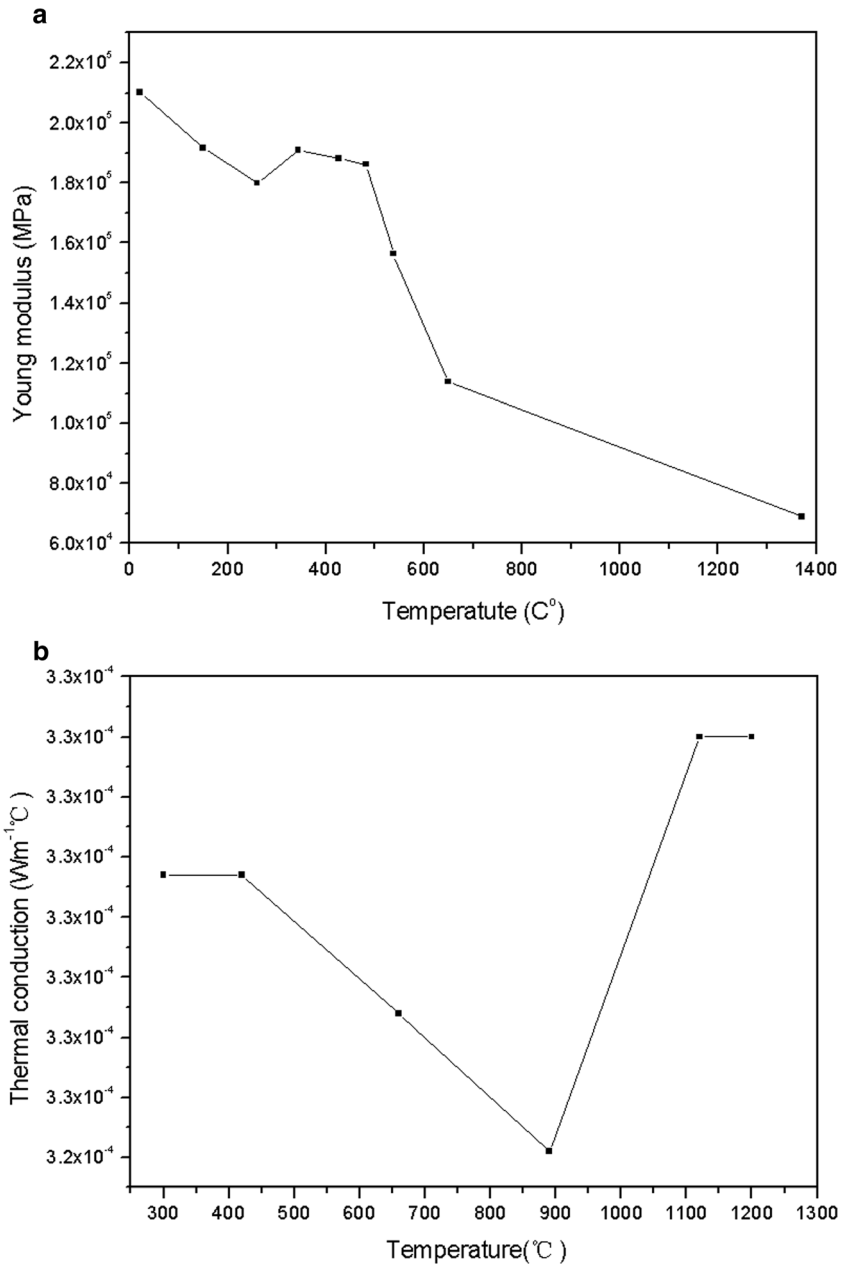

Fig. 3 The material prosperities for H13 [18]: **a** H13 tool-steel with the Young's modulus; **b** temperature-dependent thermal conductivity

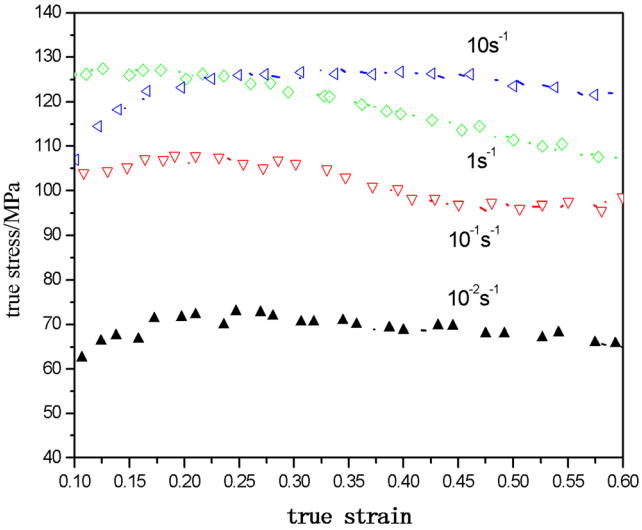

Fig. 4 True stress/true strain curves of AZ31 obtained from compression tests at 300 °C under different strain rates and corrected for deformation heating during the testing

In this paper, the ambient temperature is set as 25 °C, and preheated temperature of the ES die is 350 °C. The initial billet temperature is chosen to be at a relatively high level 370 °C without running the risk of reaching the press force limit during experiments at high ram speeds. Heat transfer coefficient between tooling and billet is 11 N/°C s mm^2, and the value of heat transfer coefficients between tooling/billet and air is 0.02 N/°C s mm^2. The emissivity coefficients of the AZ31 and H13 tool-steel are 0.12 and 0.7, respectively.

3 Experimental details

The ES extrusion ratio is 12. The billet material is the same as the material which has been used in the compression tests and numerical simulations. In order to validate the results of finite element analysis, the ES dies with channel angles 120° and 135° have been designed and manufactured to perform the actual extrusion processes. The billets and ES dies in experiments and simulations are identical. The die material, die dimensions, billet dimensions, and extrusion conditions are all the same as those used in numerical simulation as described above. Before extrusion, the billets have been machined into rods with diameter of 80 mm. Real ES process have been carried out by employing a 500-MN press. ES process experiments have been carried out with a resistance-heated container and a heater. The billet has been heated in an external furnace up to 370 °C and moved into the ES die which has been preheated to 350 °C. Ram speed is 20 mm/s during experimental verification.

Table 2 Physical properties of the AZ31 workpiece

Property	AZ31
Heat transfer coefficient between tooling and billet (N/°C s mm^2)	11
Heat transfer coefficient between tooling/billet and air (N/°C s mm^2)	0.02
Poisson's ratio	0.35
Coefficient of linear expansion	26.8E−6
Density	1,780 kg/m^3
Poisson's ratio	0.35
Young's modulus	45,000 MPa
Emissivity	0.12

4 Results and discussions

4.1 The distributions of effective stress and strain during ES process

Examination of the predicted strains provided quantitative insight into the deformation behaviors of billet during ES process [20]. Figure 5 shows the effective strains contours of billets during ES process, which could provide the important information regarding the strains distributions. Figure 5a, b presents the distributions of the equivalent stress and strain for time 1.3 s when the channel angles are 120° and 135°, respectively. The effective stresses of the material are not even seen from Fig. 5a, c, and the maximum effective stress is about 165.6 MPa at time 2.5 s. It can be seen that the stress distribution is very complicated, and there is only compressive stress in the workpiece. The deformation of the initial extrusion is nonuniform, and the highest stress (254.2 MPa) from Fig. 5b is located at compression zone. Strains distributions are lamellar with distinct deformation gradients in the deformation zone. The deformation of this position is close to the simple shear deformation.

The equivalent strains during ES process have been analyzed according to Fig. 6a, b which shows regional gradients of strain distributions along the X-direction. The ranges of effective strains are 0.044–1.78 and 0.044–1.649, respectively. The maximum strains in the whole workpiece can be found in the plastic deformation zone. The total effective strains in the extruded workpieces after ES process have been given, and the principle of ES process is to introduce compressive and shear strain into the workpieces. The characters of ES process are that the sample is subjected to direct extrusion and twice shear deformation. The accumulative strain of ES process can be expressed as Eq. (1) [21–24] which include accumulative strains of direct extrusion and two continuous shears steps.

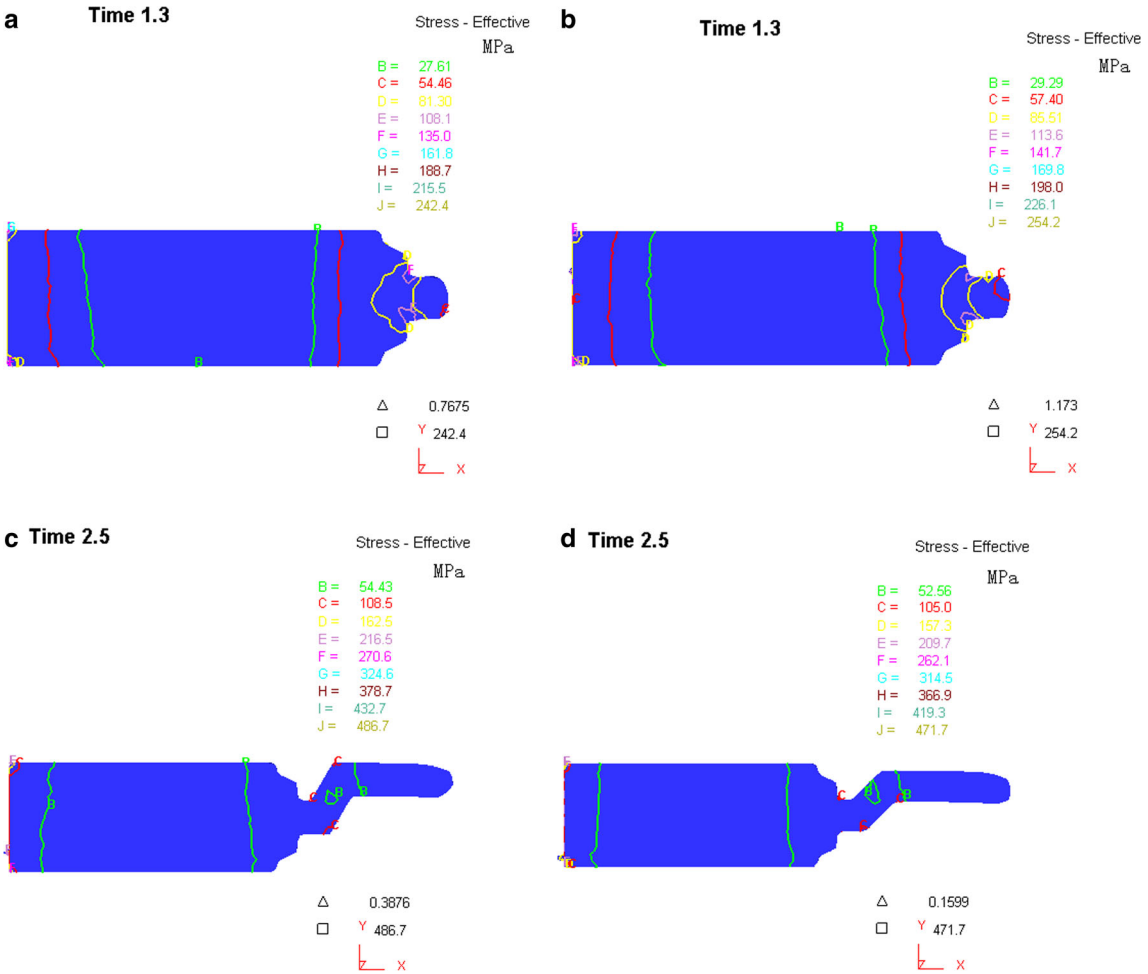

Fig. 5 The distributions of equivalent stresses distribution: **a** extrusion time 1.3 s for ES die with channel angle 120° and **b** 135°; **c** extrusion time 2.5 s for ES die with channel angle 120° and **d** 135°

$$\varepsilon = \ln\lambda + 2 * \left[\frac{2\cot\left(\frac{\phi}{2}+\frac{\psi}{2}\right) + \psi\csc\left(\frac{\phi}{2}+\frac{\psi}{2}\right)}{\sqrt{3}}\right] \quad (1)$$

Where ε is the accumulative strain, λ the extrusion ratio the inner channel angle, and Ψ the outer channel angle.

According to Eq. (1), the cumulative effective strain is a function of die structure parameters. The average effective strain after direct extrusion in the steady-state strain region is approximately 2.48. After two steps simple shears, the cumulative effective strains of ES process for channel angles 120° and 135° of ES dies are 5.6 and 4.7, respectively. The strains caused by ES die with channel angle 120° are much higher than which caused by ES die with channel angle 135°. Channel angles of ES die have important effects on the deformation of the workpieces. Figure 7 shows the maximum and minimum effective strains with different channel angles. The maximum effective strains of billets in the workpiece decrease relatively with the increase of channel angle during ES according to cumulative maximum strains calculated by Eq. (1). From the results of simulation and theoretical calculation, the cumulative maximum strains caused by the ES die with channel angle of 120° are higher than those of the die with angle 135°. In order to improve the efficiency of accumulative deformation, ES die with channel angle 120° should be adopt. To decrease the resistance forces of ES process, the optimized channel angle is 135°.

4.2 The homogeneity of metal flow influenced by the channel angles

Optimization of the metal flow is very important which could increase the formability of metal and eliminate defects. The nonhomogeneous metal flow at the die exit causes the extrusion defects such as cracks on surface of the extrusion product. Many factors may influence the metal flow; among which, the die structure is closely related to nonhomogeneity of metal

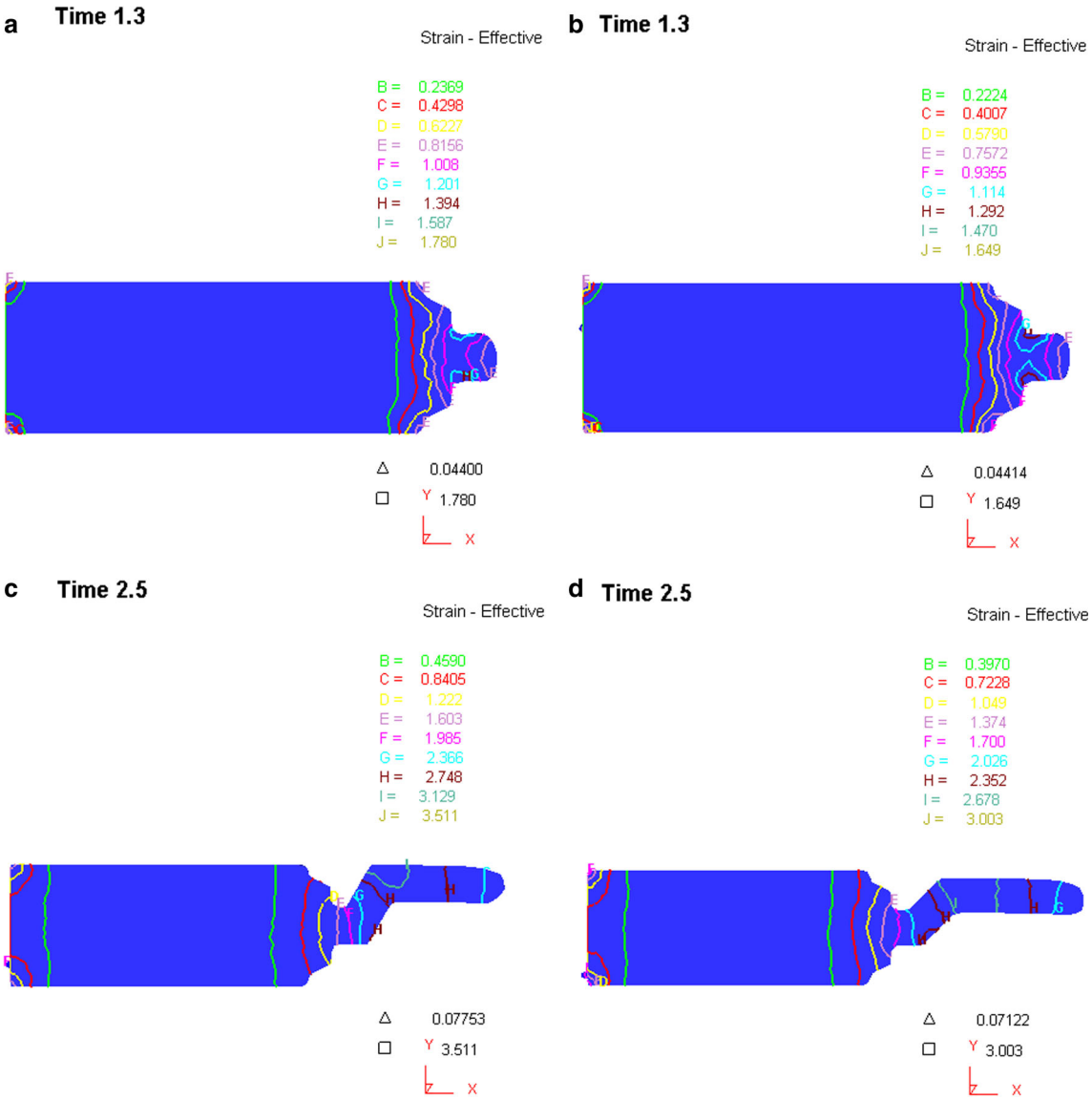

Fig. 6 The distributions of equivalent strains distribution: **a** extrusion time 1.3 s for ES die with channel angle 120° and **b** 135°; **c** extrusion time 2.5 s for ES die with channel angle 120° and **d** 135°

flow. To research the nonhomogeneity of metal flow influenced by the channel angles, some investigated points (p_1 to p_{20} shown in Fig. 8a) distributing along the radius direction at the die exit are chosen. Flow velocities along extrusion direction at the die exit with different channel angles at extrusion time 2.174 s have been illustrated in Fig. 8b.

In order to investigate the effects of die angles on homogeneity of metal flow, the mean square deviation of velocity is considered as the objective function, which is defined as Eq. [25] (2).

$$YD = \sqrt{\frac{\sum_{i=1}^{N} \left(v_{x,i} - v_{x,av}\right)^2}{N}} \tag{2}$$

where N equals 20 and i, $\nu_{x,\,j}$, and $\nu_{x,\,av}$ are the investigated point number, axial velocity of the points, and the mean axial velocity of the points, respectively.

The optimization object is to minimize the mean square deviation of velocity. In order to investigate and estimate the metal flow velocity completely and accurately, the velocity of the X and Y directions of the points shown in Fig. 8b with the channel angles 120° and 135° at the ES die exit is shown. It is clear that the ES die with channel angle 135° would cause the bigger velocity along the X-direction, and the velocities along the Y direction are lower. So the ES die with 135° channel angle could improve the forming efficiency and straight of rods.

The mean square deviation of velocities at the extrusion die exit for ES dies with channel angles 120° and 135° is shown in

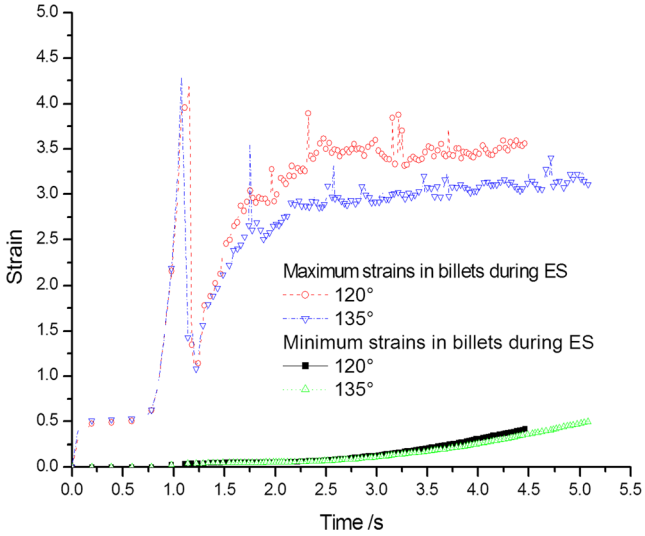

Fig. 7 The maximum and minimum strains curves under the conditions of ES dies with channel angles 120° and 135°

Fig. 8c when the extrusion steps of the top die are 100, 150, and 200, respectively. The comparisons of the mean square deviations for the X-axial velocity indicate that the metal flow at the die exit with the die angle 120° is more nonhomogeneous during whole ES process. The flow velocity at the die exit with the channel angle 120° of each point is approximate, and the discrepancy of the mean square deviation of velocity is not much, which indicates that the employment of the channel angle 120° increases the metal flow homogeneity and decreases the generation of defects such as cracks caused by the flow velocity nonhomogeneity comparing with the channel angle 135°.

4.3 The curves of load and stroke with different channel angles in the ES die

The required forces varying with time for different ES dies with channel angles 120° and 135° are described in Fig. 3. The values for maximum extrusion forces are obtained from the finite element simulation. From Fig. 9, the extrusion load curve can be divided into three stages: the extrusion upsetting stage and the direction extrusion stage and continuous shears. At the initial stage, the load increases slowly during upsetting phase. The billet is subjected to severe plastic deformation. The load increases greatly to the maximum load, this stage is not steady. But the load increases rapidly due to the work hardening which resulted from the continuous accumulation of dislocations. The increments of force become slow after 1.5 s and the force curves are almost parallel with each other and ES process is steady. During the third phase, the load oscillates about an average value about 1.6 and 1.4 MN for channel angles 120° and 135°, respectively. The values of extrusion forces are varying periodically. The load-stroke

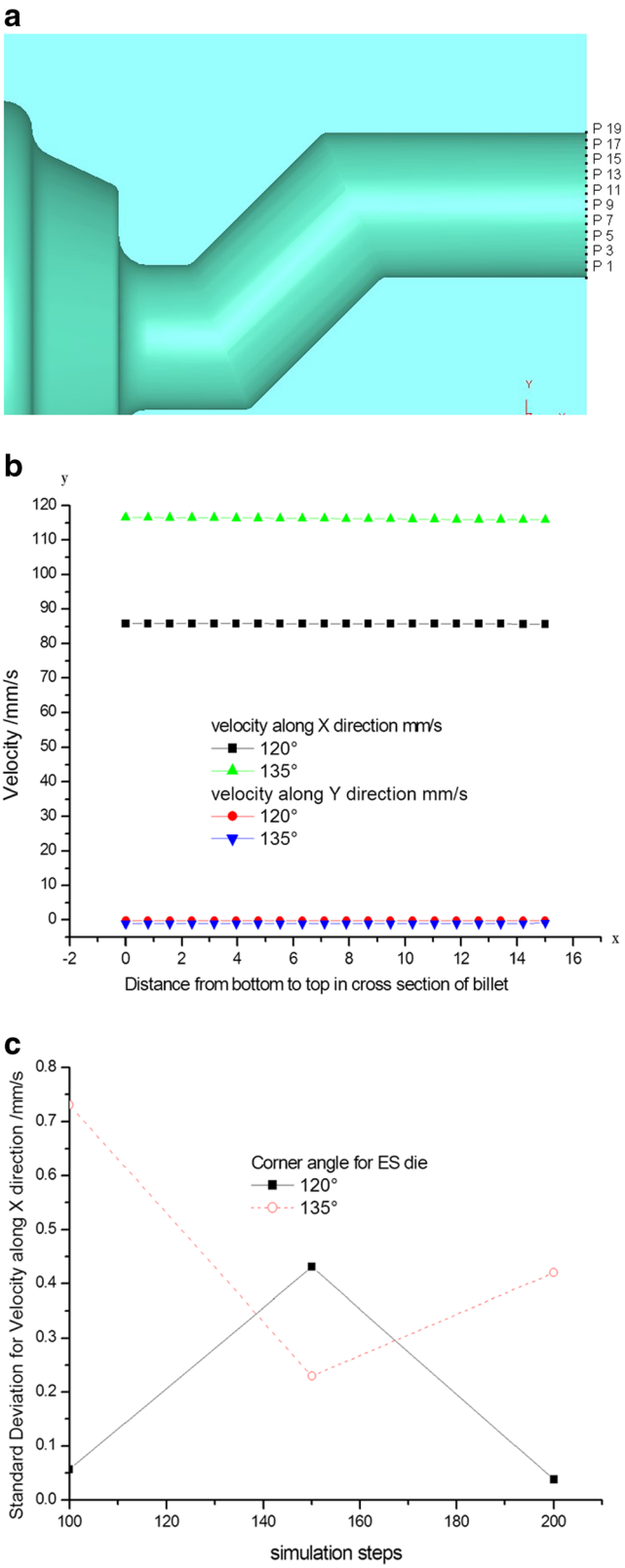

Fig. 8 Flow velocities along X-direction at the die exit with different channels angles: **a** the investigated points distributed along the radius direction at the die exit; **b** flow velocities distributions of these points; **c** curves of the mean square deviation for velocities according to the extrusion steps

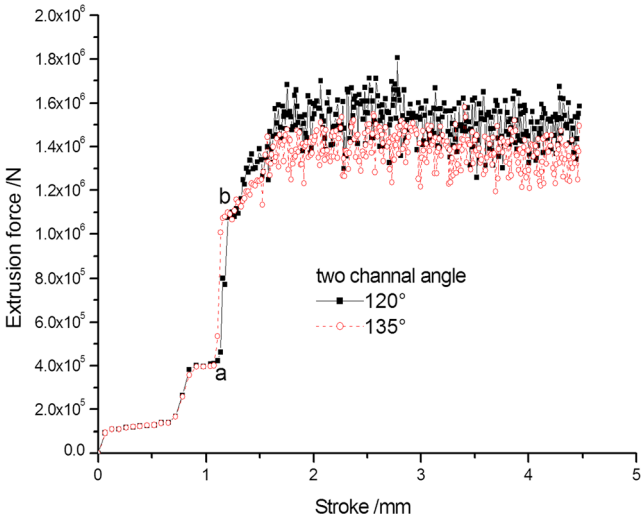

Fig. 9 Curves of load-stroke with different channels angles

curves could exhibit the characteristic of strain softening with a peak stress to a steady-state regime, which is a typical phenomenon caused by the dynamic recovery or recrystallization [26–28]. Influences of channel angles are analyzed by numerical simulation, which indicated that peak value of load increase when channel angle decreases in a near proportional relation. It should be noted that in this condition, specimen is often contacted with all the parts of the inner walls of ES die [29].

4.4 The analysis of microstructures evolution with different channel angles

Optical microstructures for ES processes with different channel angles 120° and 135° are shown in Fig. 10. There are even equiaxed grains with an average grain size of 20 μm in ES hot-extruded rods as shown in Fig. 10a, which indicate that intensive and dynamic recrystallization (DRX) has taken place during ES process when the preheated temperature of billet is 370 °C. After the hot ES process, grains are refined and more homogenous. But in Fig. 10b, there are many original grains and the sizes are more than 60 μm, the alloy grains are effectively refined by DRX [30–33]. It could be found that some tiny subgrains appear around the original coarse grains, and finer grains appear for the processing in the ES die with channel angle 120° than which caused by channel angle 135° die.

The DRX is a function of strain, strain rate, temperature, and initial grain size, which change in time. The Avrami equation [34] is used to describe the relationship between the DRXed fraction X and the effective strain.

$$X_{drex} = 1-\exp\left[-\beta_d\left(\frac{\varepsilon-a_{10}\varepsilon_p}{\varepsilon_{0.5}}\right)^{k_d}\right] \quad (3)$$

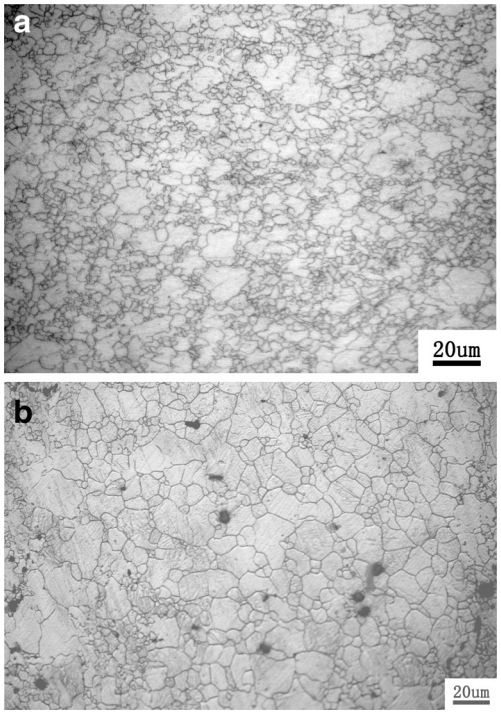

Fig. 10 Typical microstructures of extruded AZ31 Mg alloy: **a** ES die with channel angle 120°; **b** ES die with channel angle 135°

From Eq. (3), the DRXed fraction X increases with the effective strain increasing. It can be concluded that the DRXed fraction caused by ES die with angle 120° is much more than that induced by ES die with angle 135° as higher strains are produced by the former than the latter. It can be found that the accumulative strain increases with the extrusion advancing, so the grains will be refined consequently [35]. The principle of the ES process is to introduce compressive and accumulated shear strain into the sample. The character of the ES process is that the sample is subjected to twice shear deformation.

5 Conclusions

1. A FEM simulation and experiments of as-cast AZ31 Mg alloy billets subjected to ES process with channel angles 120° and 135° at 370 °C have been carried out successfully. Numerical simulation and experiments have helped in a big way understand the deformation behavior of AZ31 Mg alloy during ES process. The importance of channel angles has been realized in this study. It is found that the equivalent strains during the whole ES process decreased by increasing channel angle of ES die.
2. Deformation heterogeneity of billet during ES has been analyzed, which reveals the insufficiency of the previous 2D FEM model. The smaller channel angle could improve the deformation inhomogeneity, but reduces ES extrusion efficiency.

3. From the simulation, theoretical, and experimental results, the smaller channel angles lead to the higher cumulative strains and produce finer subgrains.
4. The loads of ES extrusion decrease mainly with the increase of channel angles. The main function of the channel angle is the effect of strain distribution.
5. The ES die with the channel angle 120° is better to improve the plasticity and deformation homogeneity of the billets made of AZ31 Mg alloy in comparison with the ES extrusion by channel angle 135° if the extrusion force is enough.

Acknowledgments This work was supported by the National Science Foundation of China (Grant No. 51101176), the open fund for Key Laboratory of Manufacture and Test Techniques for Automobile Parts (Chongqing University of Technology) Ministry of Education in 2013, the foundation of the post doctorate in Chongqing City and Project Number Xm201327, the China Postdoctoral Science Foundation funded project, and Natural Science Foundation Project of cstc2014jcyjA50004.

References

1. Segal VM, Reznikov VI, Drotyshevkij AE (1981) Plastic working of metals by simple shear. Russ Metall 1:99–105
2. Iwahashi Y, Horita Z, Nemoto M, Langdon TG (1998) The process of grain refinement in equal-channel angular pressing. Acta Mater 46: 17–31
3. Raghavan S (2001) Computational simulation of the equal-channel angular extrusion process. Scr Mater 44:91–96
4. Jiang H, Fan Z, Xie C (2007) 3D finite element simulation of deformation behavior of CP-Ti and working load during multi-pass equal channel angular extrusion. Mater Sci Eng A 485:409–414
5. Gong X, Li H, Kang SB, Cho JH, Li S (2010) Microstructure and mechanical properties of twin-roll cast Mg-4.5Al-1.0Zn alloy sheets processed by differential speed rolling. Mater Des 31:1581–1587
6. Gong X, Kang SB, Li S, Cho JH (2009) Enhanced plasticity of twin-roll cast ZK60 magnesium alloy through differential speed rolling. Mater Des 30:3345–3350
7. Matsuyama K, Miyahara Y, Horita Z, Langdon TG (2003) Developing superplasticity in a magnesium alloy through a combination of extrusion and ECAP. Acta Mater 51:3073–3084
8. Matsubara K, Miyahara Y, Horita Z, Langdon TG (2004) Achieving enhanced ductility in a dilute magnesium alloy through severe plastic deformation. Metall Mater Trans A 35A:1734–1744
9. Orlov D, Raab G, Lamark TT, Popov M, Estrin Y (2011) Improvement of mechanical properties of magnesium alloy ZK60 by integrated extrusion and equal channel angular pressing. Acta Mater 59:375–385
10. Hu HJ, Zhang DF, Zhang JP (2010) Microstructures in an AZ31 magnesium alloy rod fabricated by a new SPD process based on physical simulator. Trans Nonferrous Met Soc China 3:478–483
11. Kong F, Ma J, Kovacevic R (2011) Numerical and experimental study of thermally induced residual stress in the hybrid laser–GMA welding process. J Mater Process Technol 211:1102–1111
12. Ma J, Kong F, Kovacevic R (2012) Finite-element thermal analysis of laser welding of galvanized high-strength steel in a zero-gap lap joint configuration and its experimental verification. Mater Des 36: 348–358
13. Ma J, Kong F, Carlson B, Kovacevic R (2013) Two-pass laser welding of galvanized high-strength dual-phase steel for a zero-gap lap joint configuration. J Mater Process Technol 213(3):495–507
14. Hu H, Yang M, Gong X, Li G (2006) Optimization of casting processes based on computer numerical simulation. Ordnance Mater Sci Eng 29:51–53
15. Gong X, Anderson T, Chou K (2014) Review on powder-based electron beam additive manufacturing technology. Manuf Rev 1: 1–12
16. Gong X, Cheng B, Price S, Chou K (2013) Powder-bed electron-beam-melting additive manufacturing: powder characterization, process simulation and metrology. ASME District F-ECTC 2013: Early Career Technical Conference, Birmingham, Alabama, USA, November 2–3, 59–66
17. Qin F, Gong X, Chou K (2011) Size effects in cutting with a diamond-coated tool. Proceedings of the ASME 2011 International Manufacturing Science and Engineering Conference, Corvallis, OR, USA, June 13–17, 267–273
18. Hu HJ, Huang WJ (2013) Studies on wears of ultrafine-grained ceramic tool and common ceramic tool during hard turning using Archard wear model. Int J Adv Manuf Technol 69:31–39
19. Jiang JF, Wang Y, Qu JJ, Du ZM, Luo SJ (2010) Preparation and thixoforging of semisolid billet of AZ80 magnesium alloy. Trans Nonferrous Met Soc China 20:1731–1736
20. Li RX, Li RD, Bai YH, Qu YD, Yuan XG (2010) Effect of specific pressure on microstructure and mechanical properties of squeeze casting ZA27 alloy. Trans Nonferrous Met Soc China 20:59–63
21. Figueiredo RB, Cetlin PR, Langdon TG (2007) The processing of difficult-to-work alloys by ECAP with an emphasis on magnesium alloys. Acta Mater 55:69–79
22. Hu HJ, Fan JZ, Zhai ZY, Wang H, Li YY, Gong XB (2014) Physical fields evolution and microstructures for compound extrusion of AZ31 magnesium alloy. Russian J Non-Ferrous Metals 55:254–262
23. Hu HJ, Huang WJ (2013) Effects of turning speed on high-speed turning by ultrafine-grained ceramic tool based on 3D finite element method and experiments. Int J Adv Manuf Technol 67:907–915
24. Mofid MA, Abdollah-zadeh A, Hakan Gür C (2014) Investigating the formation of intermetallic compounds during friction stir welding of magnesium alloy to aluminum alloy in air and under liquid nitrogen. Int J Adv Manuf Technol 71:1493–1499
25. Feng F, Huang S, Hu J, Meng Z, Lei Y (2013) Analysis of the bulging process of an AZ31B magnesium alloy sheet with a uniform pressure coil. Int J Adv Manuf Technol 69(5–8):1537–1545
26. Wu G, Hu H, Gong X, Zhang W, Wang K, Dong T (2007) Application and development of casting process parameterized graph library based on AutoCAD software. Foundry Technol 28:535–537
27. Wu ZG, Song M, He YH (2009) Effects of Er on the microstructure and mechanical properties of an as-extruded Al–Mg alloy. Mater Sci Eng A 504:183–187
28. Song M, He Y, Wu Z, Huang B (2009) Multi-scale model for the ductility of multiple phase materials. Mech Mater 41:622–633
29. Song M, Wu Z, He Y (2008) Effects of Yb on the mechanical properties and microstructures of an Al–Mg alloy. Mater Sci Eng A 497:519–523
30. Qian Z, Chumbley LS, Misra S, Miller G, Pecharsky VK, Gschneidner KA, Ahn K, Chernyshov AS, Singh NK (2009) Electron microscopy examination of R5T4 alloys, where R = Ho, Yb and Gd, and T = Si, Ge, Ga and Sb. Acta Mater 57:3374–3381
31. Cao Q, Chumbley LS, Qian Z (2010) Thermal stability of RE5 (SixGe1 − x)3 plates in RE5(SixGe1 − x)4 alloys, where RE = Gd and Ho. Intermetallics 18:1021–1026

32. Qian Z, Chumbley S, Johnson E (2011) The effect of specimen dimension on residual stress relaxation of carburized and quenched steels. Mater Sci Eng A 529:246–252
33. Qian Z, Chumbley S, Karakulak T, Johnson E (2013) The residual stress relaxation behavior of weldments during cyclic loading. Metall Mater Trans A 44:3147–3156
34. Rajakumar S, Razalrose A, Balasubramanian V (2013) Friction stir welding of AZ61A magnesium alloy. Int J Adv Manuf Technol 68(1–4):277–292
35. Pan FS, Zhang J, Wang JF, Yang MB, Han EH, Chen RS (2010) Key R&D activities for development of new types of wrought magnesium alloys in China. Trans Nonferrous Met Soc China 20:1249–1258